Received: 25 June 2021 | Revised: 12 August 2021 | Accepted: 31 August 2021

DOI: 10.1096/fj.202101066R

THE FASEB JOURNAL

RESEARCH ARTICLE

Disease mechanisms of X-linked cone dystrophy caused by missense mutations in the red and green cone opsins

Ping Zhu[1] | **Frank Dyka**[1] | **Xiaojie Ma**[1] | **Ling Yin**[1] | **Heather Yu**[1] | **Wolfgang Baehr**[2,3,4] | **William W. Hauswirth**[1] | **Wen-Tao Deng**[1]

[1]Department of Ophthalmology, University of Florida, Gainesville, Florida, USA

[2]Department of Ophthalmology, John A. Moran Eye Center, University of Utah Health Science Center, Salt Lake City, Utah, USA

[3]Department of Neurobiology and Anatomy, University of Utah Health Science Center, Salt Lake City, Utah, USA

[4]Department of Biology, University of Utah, Salt Lake City, Utah, USA

Correspondence
Wen-Tao Deng, Department of Ophthalmology and Visual Sciences, West Virginia University, 1 Medical Center Drive, Box 9193, Morgantown, WV 26506, USA.
Email: wen.deng@hsc.wvu.edu

Present address
Wen-Tao Deng, Department of Ophthalmology and Visual Sciences, West Virginia University, Morgantown, West Virginia 26501, USA and Department of Biochemistry, West Virginia University, Morgantown, West Virginia 26501, USA

Funding information
National Institutes of Health, Grant/Award Number: R01 EY030056, EY021721, R01 EY08123 and 1S10OD028476; National Eye Institute, Grant/Award Number: EY014800-039003; Research to Prevent Blindness; National Institutes of Health, Grant/Award Number: R01 EY030056, EY021721, R01 EY08123 and 1S10OD028476

Abstract

Cone photoreceptors are responsible for the visual acuity and color vision of the human eye. Red/green cone opsin missense mutations N94K, W177R, P307L, R330Q, and G338E have been identified in subjects with congenital blue cone monochromacy or color-vision deficiency. Studies on disease mechanisms due to these cone opsin mutations have been previously carried out exclusively in vitro, and the reported impairments were not always consistent. Here we expressed these mutants via AAV specifically in vivo in M-opsin knockout mouse cones to investigate their subcellular localization, the pathogenic effects on cone structure, function, and cone viability. We show that these mutations alter the M-opsin structure, function, and localization. N94K and W177R mutants appeared to be misfolded since they localized exclusively in cone inner segments and endoplasmic reticulum. In contrast, P307L, R330Q, and G338E mutants were detected predominately in cone outer segments. Expression of R330Q and G338E, but not P307L opsins, also partially restored expression and correct localization of cone PDE6α' and cone transducin γ and resulted in partial rescue of M-cone-mediated light responses. Expression of W177R and P307L mutants significantly reduced cone viability, whereas N94K, R330Q, and G338E were only modestly toxic. We propose that although the underlying biochemical and cellular defects caused by these mutants are distinct, they all seem to exhibit a dominant phenotype, resembling autosomal dominant retinitis pigmentosa associated with the majority of rhodopsin missense mutations. The understanding of the molecular mechanisms

Abbreviations: adRP, autosomal dominant retinitis pigmentosa; BCM, blue cone monochromacy; ER, endoplasmic reticulum; ERG, electroretinography; GNGT2, cone transducin γ subunit; PDE6α', phosphodiesterase α subunit; UPR, unfolded protein response; WT, wild-type.

Ping Zhu, Frank Dyka, Xiaojie Ma and Ling Yin contributed equally to this work.

associated with these cone opsin mutants is fundamental to developing targeted therapies for cone dystrophy/dysfunction.

KEYWORDS

blue cone monochromacy, cone dystrophy, cone opsin, disease mechanism, photoreceptors

1 | INTRODUCTION

In the human retina, L- (long wavelength, *OPN1LW*) and M- (middle wavelength, *OPN1MW*) cones constitute about 95% of the total cone population and are primarily concentrated in the central macula responsible for our daylight, color, and fine spatial acuity vision.[1–4] X-linked retinal diseases resulting from mutations in the L- and M-opsin genes are associated with a wide range of visual defects including red–green color vision deficiencies (MIM 303800, MIM 303900), X-linked cone dystrophy (MIM 303700), X-linked cone dysfunction (MIM 300843), and blue cone monochromacy (MIM 303700).[5–19]

The *OPN1LW* and *OPN1MW* genes are clustered on the X-chromosome at Xq28 in a head to tail tandem arrangement with a single *OPN1LW* gene in a 5′ position followed by one or more *OPN1MW* genes.[4] These genes are likely to have derived from unequal recombination on the X-chromosome and therefore demonstrate 98% identity at the DNA coding sequence. The high sequence homology and close genomic proximity predispose the two pigment genes to relatively frequent unequal recombination and gene conversion resulting in gene deletions, duplications, or hybrid genes that consist of portions of both red and green pigment genes.[10,20,21] While most inherited red/green color vision defects described thus far are associated with rearrangements within the OPN1LW/MW gene array, a small percentage of these defects are also caused by missense mutations and intermixing of OPN1LW/MW sequences within exon 3.[11,18,22,23] These mutations cause a variety of serious cone defects, including blue cone monochromacy (BCM), X-linked cone dystrophy/dysfunction, and high myopia with abnormal cone function.[6,10,11,18,22–31]

Cone opsin missense mutations C203R, W177R, and P307L have been shown to cause congenital BCM. Patients carrying these mutations display significant disruption of retinal lamination and cone mosaic topography.[10,25,32] In tissue culture cells, C203R, W177R-encoded cone opsins were misfolded and accumulated in the endoplasmic reticulum (ER).[10,33] It was therefore hypothesized that they cause ER stress and toxicity in cone photoreceptors, leading to progressive apoptosis, similar to misfolded rhodopsin mutants.[34,35] The P307L mutant expressed in vitro showed normal glycosylation and transport to the cell membrane, however, light absorption at the appropriate wavelength and cone phototransduction were impaired. Based on its conservation in rhodopsin, P307L is predicted to alter the structure of the retinal binding pocket.[36]

Cone opsin missense mutants N94K, R330Q, and G338E have been identified in subjects of color-vision deficiency.[37] When these mutants were expressed in cultured COS-7 cells, N94K and G338E resulted in absence of absorbance and R330Q gave a low absorbance spectrum with a λ_{max} of 530 nm.[37] However, in a separate study, it was found that the N94K mutant binds the chromophore by means of an unprotonated Schiff base linkage, and the R330Q mutant showed decreased transducin activation but maintained similar thermal and chemical stabilities as normal green cone opsin.[38]

Since studies on disease mechanisms due to these cone opsin mutations have been exclusively carried out in vitro, the full impact of these mutations on cone structure and their physiological consequences are not well understood in their full normal environment. We selected *Opn1mw*$^{-/-}$ mice with abolished M-cone function for our in vivo studies. Their dorsal *Opn1mw*$^{-/-}$ cones which are normally dominated by M-opsin expression have shortened outer segments, whereas their ventral S-opsin dominant cones retain normal S-cone function and structure.[39] We expressed cone opsin mutants N94K, W177R, P307L, R330Q, and G338E specifically in *Opn1mw*$^{-/-}$ cones via AAV vectors to investigate their pathogenic effects on cone structure, function, and cone viability. N94K and W177R mutants mislocalize to cone inner segments and ER, whereas P307L, R330Q, and G338E mutants trafficked normally to cone outer segments. Our well-developed AAV vector technology targeting cones provide a powerful tool allowing us to study disease mechanisms of cone opsin mutants in vivo. The results of our study are fundamental to delineating future effective treatment strategies and to suggest the most useful knock-in mouse models for further study.

2 | MATERIALS AND METHODS

2.1 | Animals

All mice used in this study were maintained in the University of Florida Health Science Center Animal Care

Service Facilities on a 12 h/12 h light/dark cycle. All animals were maintained under standard laboratory conditions (18–23°C, 40%–65% humidity) with food and water available ad libitum. All experiments were approved by the Institutional Animal Care and Use Committee at the University of Florida and conducted in accordance with the ARVO Statement for the Use of Animals in Ophthalmic and Vision Research and National Institutes of Health regulations. M-opsin knockout (*Opn1mw*$^{-/-}$) mice have been described previously.[40] Both hemizygous males and homozygous females were used in this study. We have shown previously that there are no differences in retinal structure, morphology of cone photoreceptors, scotopic or photopic ERG responses between *Opn1mw*$^{-/-}$ hemizygous males and homozygous females.[39,40]

2.2 | Cloning of AAV vectors expressing human *OPN1LW* mutants

The human L-opsin missense mutations were generated by Q5® site-directed mutagenesis kit (New England Biolabs, Ipswich, MA, USA) following the manufacture's instruction, using our previous plasmid containing OPN1LW cDNA with an HA tag fused in a frame at the C-terminals. Each mutant was then cloned into the AAV vector under PR2.1 promoter[41] and their sequences were confirmed by sequencing. This vector was packaged in serotype 8 Y733F by transfection of H293 cells and was purified according to previously published methods.[42]

2.3 | Subretinal injections

Eyes of 1-month-old *Opn1mw*$^{-/-}$ mice were dilated with Tropi-Phen (phenylephrine HCL 2.5%, Tropicamide 1% Oph. Solution, Pine Pharmaceuticals, Tonawanda, NY 14150) 15–30 min before injection. Trans-corneal subretinal injections were performed with a 33-gauge blunt end needle attached to a 5 ml Hamilton syringe. First, an entering puncture was introduced at the edge of the cornea with a 26-gauge disposable needle, then 1 μl of viral vector mixed with fluorescein dye (0.1% final concentration) was injected through the corneal opening and delivered into the subretinal space as described previously.[43,44] An injection was considered successful if it detached at least 80% of the retina visualized by the fluorescence bleb monitored by a video camera attached to the injection scope allowing real-time assessment of surgical procedures. Atropine eye drops (Alcon, Inc. Lake Forest, IL) and neomycin/polymyxin B/dexamethasone ophthalmic ointment (Bausch & Lomb Inc. Tampa, FL, USA) were applied after injection. One eye was injected, whereas the contralateral eye was uninjected and served as a control, 5×10^9 vector genomes (vg) in 1 μl were injected. Antisedan (Orion Corporation, Espoo, Finland) at 1 mg/kg was given intramuscularly following injection as an anesthetic reversal. We also performed PBS buffer injection in *Opn1mw*$^{-/-}$ mice and observed no changes in cone structures (Figure S1). We performed AAV5-GFP injections in *Opn1mw*$^{-/-}$ mice in our previous study[40] and observed no adverse effects.

2.4 | Western blot analysis

Retinas from uninjected *Opn1mw*$^{-/-}$ mice, *Opn1mw*$^{-/-}$ mice injected with each mutant, and wild-type controls (three of each) were carefully dissected. Each sample was homogenized by sonication in 300 μl buffer containing 0.23 M sucrose, 2 mM EDTA, 5 mM Tris–HCl (pH 7.5), and cOmplete™ protease inhibitors (Millipore Sigma, Burlington, MA, USA). After centrifugation, supernatant was collected, and protein concentration was measured by a Pierce™ BCA Protein Assay Kit. Aliquots of the retinal extracts containing equal amounts of protein (40 μg) were analyzed by electrophoresis on 4%–15% Mini-PROTEAN® TGX™ Precast Gels (Bio-Rad, Hercules, CA, USA). For glycosylation analysis, retinal extracts were either left untreated or treated with the PNGase F enzyme kit (cat # P0704S; New England Biolabs, Ipswich, MA, USA) to remove the N-linked glycosaccharides. An 18 μl sample of retina extract (40 μg total protein) was mixed with 2 μl of Glycoprotein denaturing buffer, 4 μl of Glycobuffer 2, 4 μl of 10% Nonidet P40, 2 μl (1000 U) of PNGase F, and 10 μl of water, and incubated at room temperature for 1 h. The proteins were then transferred to Immobilon-FL membrane (Millipore Sigma, Burlington, MA, USA) and probed with the anti-red/green opsin antibody (Millipore, AB5405, 1:1000 dilution) or anti-HA antibody (cat # 3724, 1:3000 dilution; Cell Signaling Technology, Danvers, MA, USA). The mouse monoclonal anti-alpha tubulin (cat # T5168, 1:5000; Millipore Sigma, Burlington, MA, USA) was used as a loading control. Visualization of specific bands was performed using an Odyssey Infrared Fluorescence Imaging System (LICOR Biosciences, Lincoln, NE, USA). Protein quantification was performed with Empiria Studio® Software paired with Odyssey Imager. Protein levels of each mutant, wild-type, and *Opn1mw*$^{-/-}$ uninjected controls were normalized to α-tubulin. Data were presented as the average ± SEM from three independent immunoblots. Statistical analysis was performed with one-way ANOVA followed by Dunnett's multiple comparisons test (GraphPad Prism) to compare mutant injected eyes vs uninjected and wild-type controls. Significance was defined as a p value of $< .05$.

2.5 | Electroretinography

Cone ERG responses were analyzed using an UTAS Visual Diagnostic System with a Big Shot Ganzfeld dome (LKC Technologies, Gaithersburg, MD, USA). All ERGs were performed at 2 months postinjection. Mice were anesthetized with an intraperitoneal injection of ketamine (72 mg/kg) and xylazine (4 mg/kg). The pupils were dilated with Tropi-Phen. All animals were light-adapted before ERG to suppress any rod responses and ERG responses were never detected from contralateral untreated *Opn1mw*$^{-/-}$ eyes under photopic conditions when we performed M-cone ERGs.

Mutant-mediated cone ERGs were recorded by stimulation with green channel middle wavelength light (530 nm) at intensities of −0.6, 0.4, and 1.4 log cd s/m^2, followed by red channel long-wavelength light (630 nm) at intensities of −0.6, 0.4, and 1.4 log cd s/m^2. Twenty-five recordings were averaged for each light intensity. Stimulation with both wavelengths produced similar ERG results, and responses from green light were used to plot the figure and for statistical analysis. Short wavelength ERGs (360 nm) for measuring S-cone function were recorded at intensities of −0.6 and 0.4 log cd s/m^2. ERG data were presented as average ± SD ($n = 8$ for each mutant injected group). Statistical analysis was performed by one-way ANOVA followed by Dunnett's multiple comparisons test (GraphPad Prism) to compare mutant injected eyes vs. untreated and wild-type controls. Significance was defined as a p value of $< .01$.

2.6 | Frozen retinal section preparation and immunohistochemistry

Mice were sacrificed and their eyes were marked at 12 o'clock on the cornea with a burn marker and enucleated. A hole was introduced on the cornea by an 18-gauge needle and eyes were immersed in 4% paraformaldehyde in phosphate-buffered saline (PBS, pH 7.4) at room temperature for 2 h, the cornea and lens were then removed without disturbing the retina. The eyecups were then rinsed with PBS and cryoprotected with 30% sucrose overnight at 4°C, then embedded in cryostat compound (Tissue TEK OCT, Sakura Finetek, Torrance, CA, USA) and frozen at –80°C. Retinas were sectioned perpendicularly from dorsal to ventral at 12 μm thickness. For immunohistochemistry, retinal sections were rinsed in PBS and blocked in 3% BSA, 0.3% Triton X-100 in PBS for 1 h at room temperature. Sections were then incubated with primary antibodies at 4°C overnight. The following primary antibodies were used: anti-L/M-opsin, anti-S-opsin (MilliporeSigma, AB5405 and AB5407, respectively, 1:1000 dilution for both), anti-HA (Roche, rat monoclonal, clone 3F10, 1:200, Basel, Switzerland), anti-PDE6α' (ABgene, AP9728c, 1:200, Portsmouth, NH, USA), and anti-cone transducin γ subunit (a gift from Dr Arshavsky's lab, Duke University). After incubation with the first antibody, the slides were washed with PBS three times, followed by incubating with IgG secondary antibodies tagged with Alexa-594 or Alexa-488 (Molecular Probes, Eugene OR) diluted 1:500 in PBS at room temperature for 2 h then washed with PBS. Sections were mounted with Vectashield Mounting Medium for Fluorescence (H-1400, Vector lab, Inc. Burlingame, CA, USA) and coverslipped. Sections were imaged with a Leica Fluorescence Microscope LAS X Widefield System. Quantification of immunohistochemistry was performed by counting positive cells of each antibody staining from three images taken from three different mice. Statistical analysis was performed with paired t-tests (GraphPad Prism) to compare dorsal cone outer segment vs. ventral cone outer segment and dorsal cone inner segment vs. ventral cone inner segment for each antibody and mutant. Significance was defined as a p value of $< .001$.

2.7 | Preparation of retinal whole mounts and PNA staining

Mice were humanely euthanized, their eyes were marked at 12 o'clock on the cornea with a burn marker. The eyes were enucleated and immersion fixed for 2 h with 4% paraformaldehyde in phosphate-buffered saline (PBS, pH 7.4) at room temperature. The cornea and lens were then removed and the entire retina was carefully dissected from the eyecup. Retinas were blocked in 3% BSA for 2 h, then labeled with Biotinylated Peanut Agglutinin (PNA) (Vector Laboratories, Burlingame, CA, USA) and S-opsin antibody (MilliporeSigma, Burlington, MA, USA) in PBS at 4°C overnight. The retinas were then washed with PBS three times, followed by incubating with Fluorescein Avidin D (Vector Laboratories, Burlingame, CA, USA) and IgG secondary antibody tagged with Alexa-594 (Molecular Probes, Eugene OR, USA) diluted 1:500 in PBS at 4°C overnight, then washed with PBS. To make flat mounts, radial cuts were made from the edges to the equator of the retina. The flat mounts were flattened on slides with a fine brush, one drop of Vectashield Mounting Medium for Fluorescence (H-1400, Vector lab, In. Burlingame, CA, USA) was applied and then covered with a coverslip. The flat mounts were imaged with a Leica Fluorescence Microscope LAS X Widefield System. Four images were taken from each flat mount, two from the dorsal area, and two from the ventral area, marked by burn mark. PNA-positive cells from each image were counted in an area that is equivalent to 0.01 mm^2 of the retina using the counting tool in Adobe Photoshop. For each cone opsin injected group, counts of eight images from four different mice (two males and two females) were average for dorsal

and ventral regions, and the SD was calculated. Statistical analysis was performed by two-way ANOVA with Tukey's multiple comparison test to compare the difference among each group for the dorsal or ventral region. Significance was defined as a p value of $< .05$.

3 | RESULTS

3.1 | Expression of cone opsin mutants in vivo

The following cone opsin missense mutants were cloned in AAV vector under the cone-specific promoter PR2.1 and packaged in a serotype 8 mutant Y733F capsid: N94K, W177R, P307L, R330Q, and G338E. Locations of these mutant residues in human OPN1MW are illustrated in Figure 1A.[45] AAV vectors expressing each of the cone opsin mutants were injected subretinally into one eye of 1-month-old *Opn1mw*$^{-/-}$ mice, whereas the contralateral eyes were uninjected and served as controls. First, we investigated the expression levels of these cone opsin mutants in *Opn1mw*$^{-/-}$ eyes by western blot analysis (Figure 1B). Uninjected *Opn1mw*$^{-/-}$ mice have no endogenous M-opsin expression. AAV-mediated expression of N94K and W177R was barely detectible, whereas P307L, R330Q, and G338E showed expression levels higher than that of endogenous M-opsin in wild-type mice by an antired/green opsin antibody raised against the C terminus of human L/M-opsins[46] (Figure S2). Since human cone opsins have been shown to be *N*-glycosylated at N-terminal residue Asn-34,[47,48] we investigated whether *N*-glycosylation of these mutants was affected. Protein extracts were treated with PNGase F to remove N-linked glycosaccharides. Following PNGase F treatment, all five mutant bands shifted to a lower molecular mass by an HA

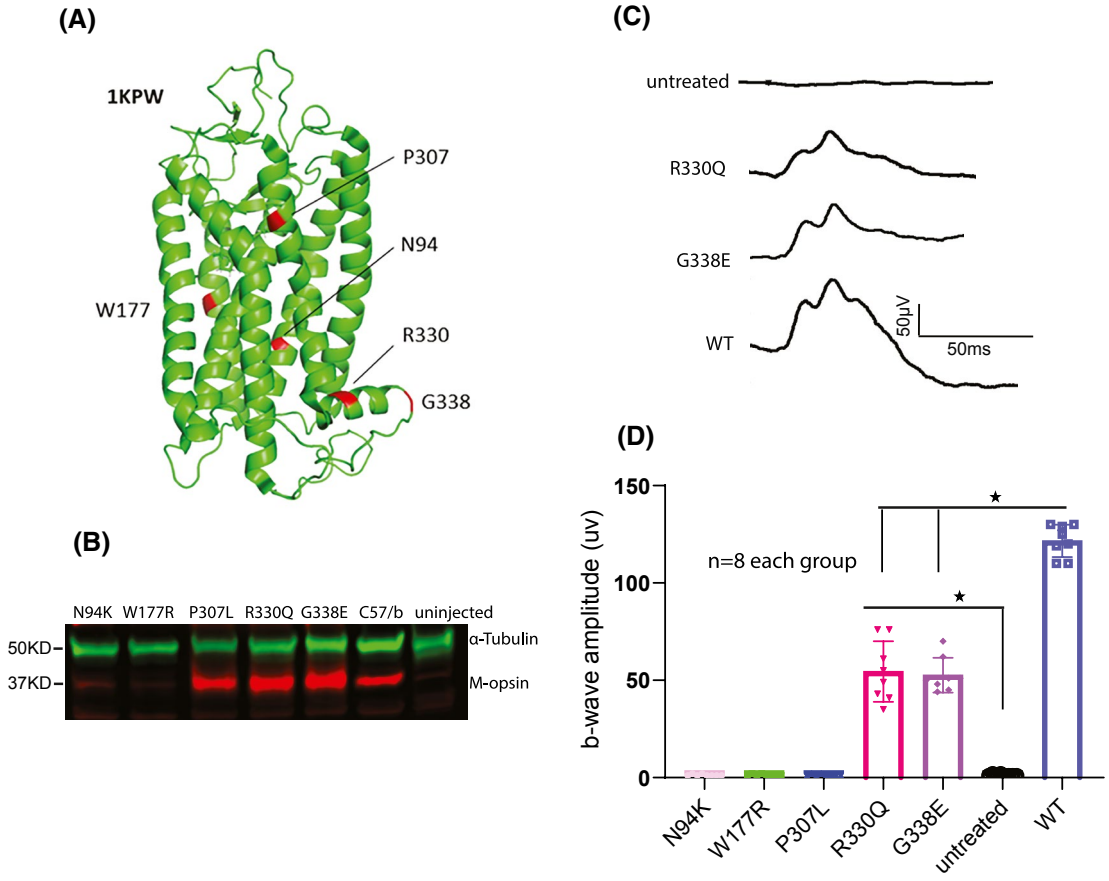

FIGURE 1 Expression and function of cone opsin mutants. (A) Location of mutant residues in human green opsin (OPN1MW, PDB ID: 1KPW; drawn with PyMOL, Molecular Graphics System, Version 1.2r3pre, Schrödinger, LLC). N94 is located in helix II, W177 in helix IV, P307 in helix VII, and R330 and G338 in C-terminal α-helix. (B) Representative immunoblot of AAV-mediated expression of cone opsin mutants in *Opn1mw*$^{-/-}$ mice at 2 months of postinjection. Anti-M-opsin (red); α-tubulin (loading control, green). Retinas from C57BL/6J and *Opn1mw*$^{-/-}$ mice were used as positive and negative controls, respectively. (C) Representative ERG traces of R330Q and G338E opsins at 1.4 log cd s/m^2 under 530 nm wavelength light. (D) Individual and averaged M-cone ERG responses from each mutant opsin injected *Opn1mw*$^{-/-}$ eye. Average represents the mean ± SD of b-wave amplitudes recorded at 1.4 log cd s/m^2 ($N = 8$ for each group, $^*p < .0001$). Untreated *Opn1mw*$^{-/-}$ and wild-type mice served as controls

antibody suggesting that *N*-glycosylation was not affected (Figure S3). N94K, W177R, and their deglycosylated forms can be detected but only after prolonged exposure. This is consistent with a previous study that glycosylation is not required for the formation of cone opsins.[49] We were not able to detect the deglycosylated bands by the L/M-opsin antibody we used.

3.2 | Light responses of missense cone opsin mutants

Next, we investigated whether any of these cone opsin missense mutants are capable of mediating light responses when expressed in *Opn1mw*$^{-/-}$ eyes. Uninjected *Opn1mw*$^{-/-}$ mice have normal S-cone mediated light response but no M-cone ERGs.[40] Of the five mutants, N94K-, W177R-, and P307L-treated eyes demonstrated no middle (530 nm) or long (630 nm) wavelength-mediated light responses, whereas R330Q and G338E showed ERG responses at both wavelengths (Figures 1C and S4). The ERG amplitudes at 530 nm in R330Q and G338E injected eyes were 54.5 ± 15.5 μV and 56.3 ± 18.1 μV, respectively (average ± SD, $n = 8$). ERG responses in both cases were significantly higher than the unrecordable ERGs from untreated contralateral control eyes ($p < .0001$) but were also significantly lower than wild-type controls (121.6 ± 8.3 μV, $n = 8$, $p < .0001$) (Figure 1D). These results suggest that R330Q and G338E, although capable of generating light responses, are defective in cone phototransduction. R330Q and G338E both are located on the C-terminal α-helix (Figure 1A). Helix 8 in rhodopsin has been shown to be important for arrestin binding.[50] In addition, cones with both arrestin 1 and arrestin 4 deleted showed significantly reduce b-wave amplitudes because the phototransduction cascade is not properly turned off.[51] Therefore, R330Q and G338E opsins could cause inefficient arrestin binding resulting in reduced b-wave amplitudes.

3.3 | Subcellular localizations of cone opsin mutants

Next, we characterized the subcellular localizations of these cone opsin mutants expressed in *Opn1mw*$^{-/-}$ eyes. Previously, we showed that the dorsal cones of *Opn1mw*$^{-/-}$ mice have significantly shortened outer segments, however, these cones remain viable. We also showed that ventral S-opsin dominant cones of *Opn1mw*$^{-/-}$ mice had normal cone structure and morphology.[39] Here we determined the subcellular localizations of each cone opsin mutant in both dorsal and ventral retinas in treated *Opn1mw*$^{-/-}$ eyes. We also examined the subcellular localization of two endogenous cone outer segment-specific proteins, phosphodiesterase α subunit (PDE6α'), and cone transducin γ subunit (GNGT2), after AAV-delivery of each mutant.

N94K (Figures 2 and S5A) and W177R (Figures 3 and S5B) opsins were exclusively detected in cone inner

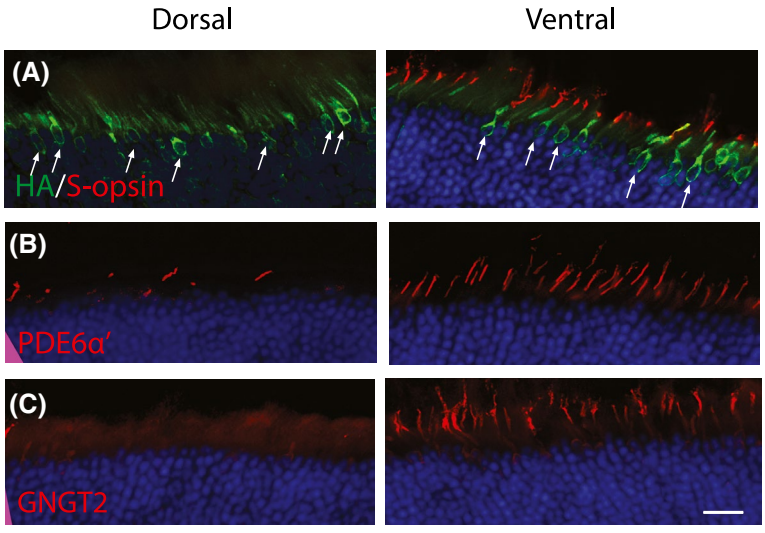

FIGURE 2 Subcellular localization of N94K opsin, PDE6α', and GNGT2 in injected *Opn1mw*$^{-/-}$ retinas. (A) N94K expression was detected by an anti-HA antibody (green). N94K opsin was misfolded and localized predominately in cone inner segments and ER (arrows) in both dorsal and ventral retinas. The rough ER (arrows), where cone opsins are synthesized, was shown as green circles surrounding the cone nucleus by HA staining. S-opsin expression (red) was mainly detected in cone outer segments in the ventral area. (B) PDE6α' was barely detectible in the dorsal area, while it was expressed normally and localized correctly in cone outer segments in the ventral area of the same eye, where S-opsin was present. (C) GNGT2 was not detected in the dorsal area, while it was expressed normally and localized in cone outer segments in the ventral area of the same eye. Scale bar: 20 μm

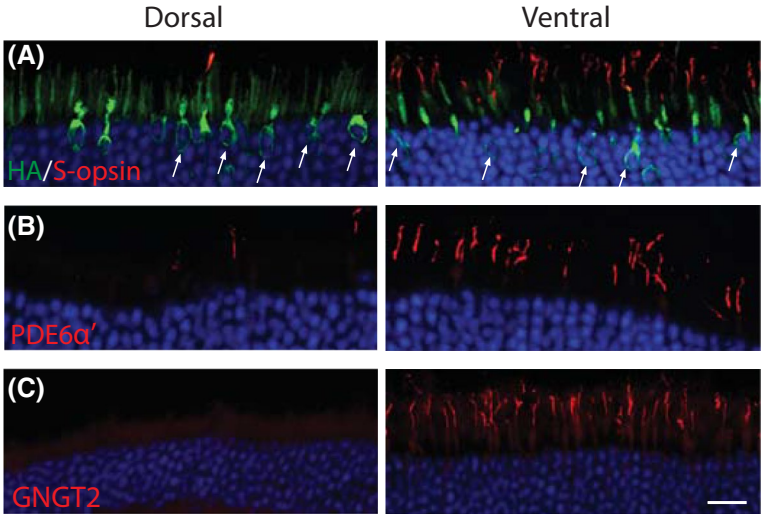

FIGURE 3 Subcellular localization of W177R opsin, PDE6α', and GNGT2 in injected *Opn1mw*$^{-/-}$ retinas. (A) W177R (green) was misfolded and localized exclusively to cone inner segments and ER (arrows) in both the dorsal and ventral retina. (B) PDE6α' was barely detectible in the dorsal area while it was expressed normally and localized to cone outer segments in the ventral area of the same eye, where S-opsin was present. (C) GNGT2 was not detected in the dorsal area, while it was expressed normally and localized to cone outer segments in ventral area. Scale bar: 20 μm

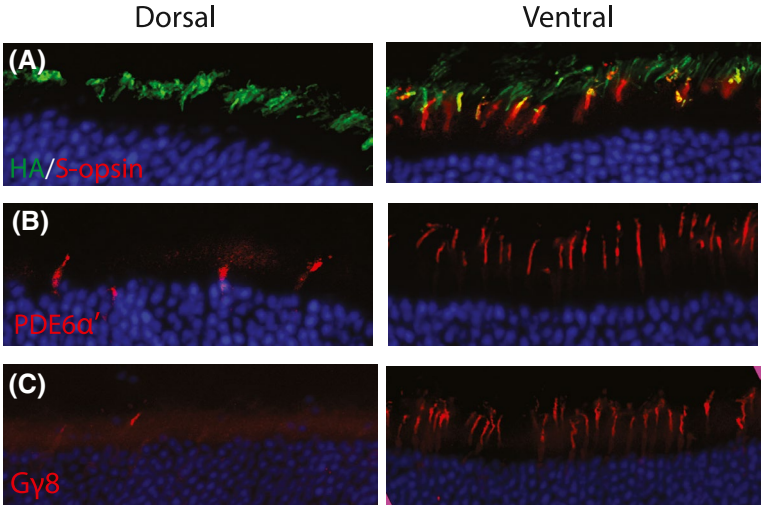

FIGURE 4 Subcellular localization of P307L opsin, PDE6α', and GNGT2 in injected *Opn1mw*$^{-/-}$ retinas. (A) P307L opsin (green) was expressed in cone outer segments in both dorsal and ventral retinas and colocalized with endogenous S-opsin in the ventral area. (B) PDE6α' expression was barely detectible in the dorsal retina, while it was expressed normally and localized in cone outer segments in the ventral area. (C) GNGT2 was also not detected in the dorsal area while expressed normally and localized to cone outer segments in the ventral area. Scale bar: 20 μm

segments and in the ER in both dorsal and ventral areas of injected *Opn1mw*$^{-/-}$ retinas. The rough ER, where cone opsins are synthesized, surrounds the cone nucleus, which was shown as green circles in the outer nuclear layer by HA staining. Antibodies against PDE6α' and GNGT2 showed that both were barely detectible in the dorsal retinas, whereas they expressed normally and localized correctly in cone outer segments in the ventral retinas of the same eye, where S-opsin was present.

In contrast to N94K and W177R, P307L was expressed in cone outer segments in both dorsal and ventral retinas (Figures 4 and S5C). However, in the dorsal area, only a few PDE6α' positive cells were detected and only in cone inner segments, and no GNGT2 expression was detected. In contrast, PDE6α' and GNGT2 were expressed normally in cone outer segments in the ventral retina of the same eye.

R330Q (Figures 5 and S5D) and G338E (Figures 6 and S5E) were both detected in cone outer segments in

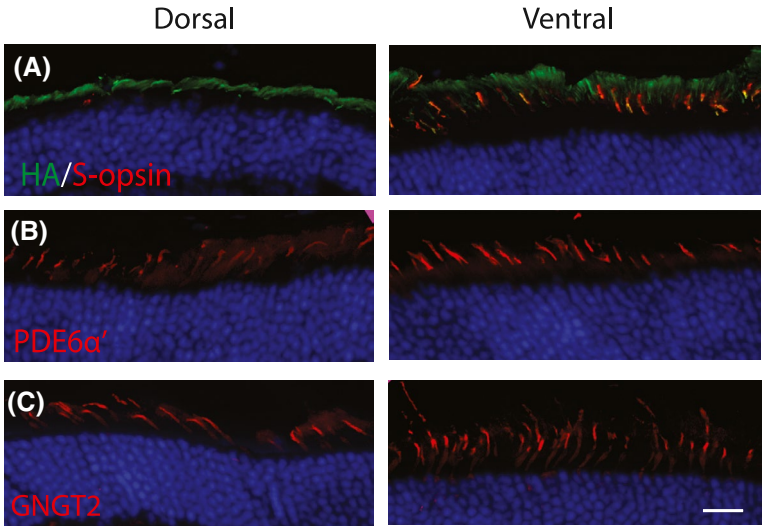

FIGURE 5 Subcellular localization of R330Q opsin, PDE6α', and GNGT2 in injected *Opn1mw*$^{-/-}$ retinas. (A) R330Q opsin (green) was expressed in cone outer segments in both dorsal and ventral retinas. (B) PDE6α' expression was partially restored in cone outer segments in the dorsal retina. (C) GNGT2 expression was also partially restored in cone outer segments in the dorsal retina. Scale bar: 20 μm

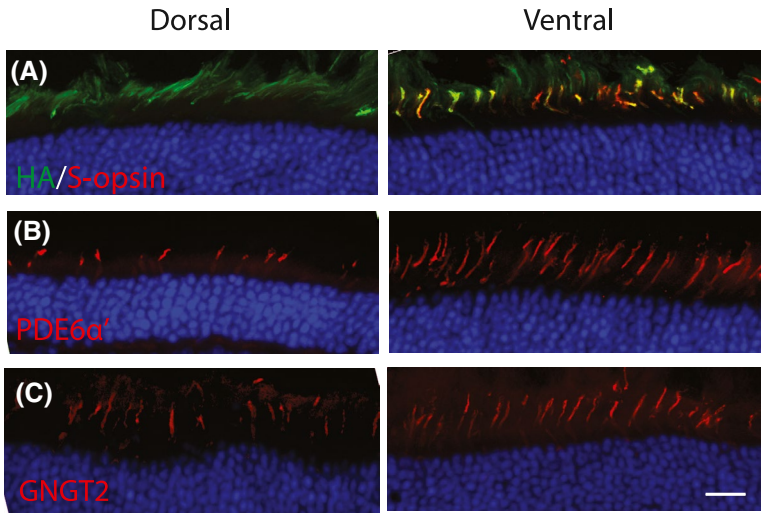

FIGURE 6 Subcellular localization of G338E opsin, PDE6α', and GNGT2 in injected *Opn1mw*$^{-/-}$ retinas by immunohistochemistry. (A) G338E opsin (green) was expressed in cone outer segments in both dorsal and ventral retinas. (B) PDE6α' expression was partially restored in cone outer segments in the dorsal retina. (C) GNGT2 expression was also partially restored in cone outer segments in the dorsal retina. Scale bar: 20 μm

injected *Opn1mw*$^{-/-}$ dorsal and ventral retinas. Moreover, in both mutants injected eyes, PDE6α' and GNGT2 expression were detected in cone outer segments in dorsal retinas, although there were fewer PDE6α'/GNGT2 stained cells and staining intensities were less in dorsal compared with ventral areas of the same eye. These results suggest that R330Q and G338E partially support cone outer segment formation in the dorsal retina. In addition, their normal targeting partially restored expression and localization of the remaining cone outer segment proteins.

3.4 | Cone viability of *Opn1mw*$^{-/-}$ eyes expressing different cone opsin mutants

We determined cone viability in *Opn1mw*$^{-/-}$ retinas expressing each cone opsin mutant. To do this, we compared numbers of peanut agglutinin (PNA) positively stained cells in both dorsal and ventral mutant-treated retinas to their contralateral, untreated eyes at 5 months postinjection (Figure 7). PNA specifically binds to the extracellular glycoprotein matrix of cone outer and inner segment sheaths and is an indicator of cone viability.[52] Each of these five mutants reduced the number of viable cones in the *Opn1mw*$^{-/-}$ retina to a varying degree. Expression of W177R and P307L led to a severe loss of viable cones and reduced the number of cells which stained positively for PNA by ~70% in dorsal retinas and ~40% in ventral retinas, compared with age-matched, untreated controls ($n = 8$, $p < .0001$). Furthermore, when N94K, R330Q, or G338E was expressed in the *Opn1mw*$^{-/-}$ retina, the number of viable cones diminished at a range of 15%–25% in both the dorsal and ventral regions. Statistical analysis showed that in some cases, these three mutants reduced viable cones moderately ($n = 8$, $p < .05$), whereas in other cases, they did not cause a significant reduction of viable cones ($n = 8$, $p > .05$).

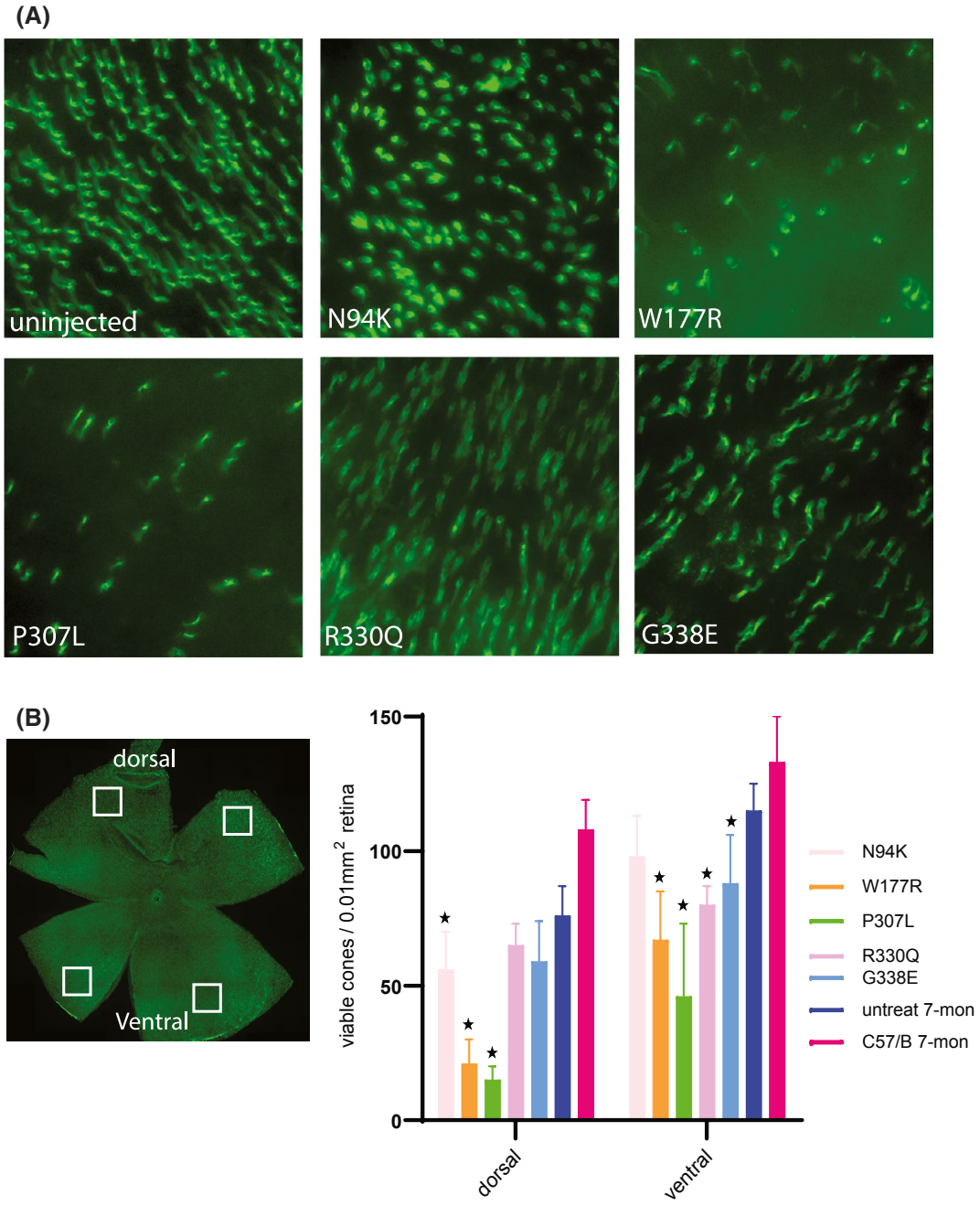

FIGURE 7 Evaluation of cone viability in *Opn1mw*$^{-/-}$ retinas expressing each cone opsin mutant. (A) Representative images were taken from dorsal areas of retinal flat mounts of *Opn1mw*$^{-/-}$ mice injected with each cone opsin mutant at 5 months of postinjection. Retinal whole mounts were stained with PNA. (B) Quantification of PNA staining from dorsal and ventral areas of retinal wholemounts of *Opn1mw*$^{-/-}$ eyes injected with different opsin mutants. Seven-month-old uninjected *Opn1mw*$^{-/-}$ and wild-type mice were used as controls. Each bar represents PNA-positive cells counted within a 0.01mm^2 surface area of the retina from eight images taken from four different mice. Data show average ± SD. *$p < .05$, when compared with untreated controls

We also measured S-cone ERG responses of the *Opn1mw*$^{-/-}$ mice injected with these mutants as a further indicator of their toxicity (Figures S4 and S6). S-cone ERG reduction caused by each mutant is consistent with toxicity evaluated by PNA staining. W177R and P307L injected eyes showed severely reduced S-cone ERG responses (27 ± 14 μV and 28 ± 14 μV, respectively, average ± SD, $n = 8$, $p < .0001$) compared with untreated *Opn1mw*$^{-/-}$ eyes (106 ± 18 μV) or wild-type controls (94 ± 16 μV). R330Q and G338E injected eyes showed modestly reduced S-cone ERG responses (75 ± 23 μV, and 59 ± 12 μV, respectively, $n = 8$, $p < .001$), whereas N94K injected eyes showed normal S-cone ERG (101 ± 18 μV, $n = 8$, $p > .05$).

4 | DISCUSSION

Currently, studies on disease mechanisms associated with cone opsin mutations have been mostly carried out in vitro, thus the full impact of these mutations on cone structure and their physiological consequences are not well understood. In this study, we characterized five cone opsin missense mutations by expressing them via AAV vectors in *Opn1mw*$^{-/-}$ mice, taking advantage of the fact that dorsal cones of *Opn1mw*$^{-/-}$ mice with shortened cone outer segments remain viable. We investigated their subcellular localization, identified the pathogenic effects of these mutants on cone structure, function and viability. Our results are fundamental to delineating future effective treatment strategies.

4.1 | These cone opsin mutants are predicted to display a dominant phenotype

There are more than 130 distinct rhodopsin mutations, most of them associated with autosomal-dominant retinitis pigmentosa (adRP).[53–58] Because L/M-opsin genes are X-linked, affected males express only the mutant copy, while in female carriers, due to X-linked inactivation, each cone cell expresses either a wild-type or a mutant copy. Therefore, it is not known whether currently identified cone opsin point mutants have a dominant-negative phenotype or not. Based on our results, although these five cone opsin mutants may display distinct biochemical and cellular defects, we predict that all may present a dominant phenotype.

The corresponding rhodopsin mutations of N94K and W177R both cause autosomal dominant retinitis pigmentosa in humans.[53,59] The cone inner segment and ER localization of N94K and W177R supports that they are misfolded and might be displaying a dominant phenotype. The corresponding rhodopsin mutations of P307L, R330Q, and G338E have not been identified. All three mutants were expressed normally and detected exclusively in the cone outer segments suggesting that they are correctly or partially correctly folded. The presence of a large quantity of mutant opsin is likely to significantly alter the physical properties, composition, and light signal properties of the cone outer segment membranes, resulting in a dominant phenotype. We summarized our findings and predictions in Table 1.

4.2 | Disease mechanisms associated with each of the cone opsin mutants

Based on the disease mechanisms associated with each mutant, these five cone opsin missense mutations can be categorized into three discrete classes. N94K and W177R are misfolded and retained in the ER, and the toxic aggregation of the misfolded mutant protein causes ER stress and may be the cause of cone cell death and a degenerative phenotype, similar to class 2 rhodopsin mutants.[53] N94K expressed in cultured COS-7 cells regenerated visual pigment after adding 11-*cis*-retinal, however, the regenerated N94K opsin was inactive.[37] The N94 residue is highly conserved among vertebrate opsins.[60] Based on the crystal structure of bovine rhodopsin, N78 (corresponding to N94 in the red/green opsin) is necessary for connecting helices II, III, and IV through hydrogen bonds. If the same hydrogen bonds are also involved in connecting helices of red/green opsins, then the N94K mutation is likely to disturb the normal folding of the protein.[37] The amino acid W177 is located within transmembrane helix IV of red and green opsins and is highly conserved in visual and nonvisual opsins across species.[60] The W177R mutation and its equivalent W161R mutation in rod opsin both result in protein misfolding and retention in the ER when expressed in vitro.[10] Our result that N94K and W177R opsins are localized to the cone inner segment and ER, and mediate no light response supports that they are misfolded, and display a dominant phenotype.

We showed that P307L opsin is glycosylated and transported to the cone outer segments. However, the P307L

TABLE 1 Summary of cone opsin mutants and predicted phenotype

Mutants	Localization	PDE6C/GNGT2 localization in dorsal retinas	M-cone ERG	Predicted phenotype	References (PMID)	Corresponding rhodopsin mutation
N94K	CIS, ER	Barely detectible	No response	Dominant	12051694; 28487225	N78I, adRP or adCSNB,
W177R	CIS, ER	Barely detectible	No response	Dominant	20579627	W161R, adRP
P307L	COS	Barely detectible	No response	Dominant	9479007; 8213841	Not found
R330Q	COS	COS	Rescue	Dominant	12051694; 28487225	Not found
G338E	COS	COS	Rescue	Dominant	12051694	Not found

Abbreviations: adCSNB, autosomal dominant congenital stationary night blindness; adRP, autosomal dominant retinitis pigmentosa; CIS, cone inner segments; COS, cone outer segments; ER, endoplasmic reticulum.

mutant mediated no light response. IHC showed no expression of PDE6α' or GNGT2 in cone outer segments in the dorsal *Opn1mw*$^{-/-}$ cones indicating that normal targeting of P307L did not restore expression or localization of the remaining cone outer segment proteins. Both dorsal and ventral cones of injected *Opn1mw*$^{-/-}$ mice showed rapid cone degeneration suggesting that P307L caused severe toxicity and led to rapid cell death. Our result is consistent with a previous in vitro study showing that P307L opsin was glycosylated and targeted to cell membranes. However, the regenerated visual pigment had a diminished ability to absorb light at the appropriate wavelengths and to activate transducin. Since P307 is located within the same transmembrane alpha-helix as K312, the site of covalent attachment of 11-cis retinal, it was proposed that the mutation disrupted the retinal-binding pocket.[36]

Both R330Q and G338E opsins were capable of targeting cone outer segments and generated light responses in *Opn1mw*$^{-/-}$ mice about 50% of levels compared with treatment with normal human L-opsin.[39] AAV-mediated delivery of R330Q and G338E cone opsins are abundantly expressed in cone outer segments, however, their expression only partially rescued expression and outer segment localization of PDE6α' and GNGT2. PDE6α' and GNGT2 were expressed in fewer cells at reduced levels in dorsal retinas compared with their counterpart of the ventral cones of the same eye. Based on this data, we speculate that the cone outer segments generated by R330Q and G338E expression had abnormal structure or shorter outer segments. Moreover, R330Q and G338E opsins may have reduced affinity for arrestin since both are located on the C-terminal α-helix. In rhodopsin, conformational changes in Helix 8 are intimately involved in the binding process of visual arrestin, and chemical modifications of H8 inhibit arrestin binding.[50] The R330Q mutant expressed in COS-1 cells showed decreased phototransduction activation but maintained similar thermal and chemical stabilities as normal green cone opsin.[38] The G338 residue is well conserved in vertebrate opsins. In vitro study showed that the corresponding rhodopsin mutant G324E gave an absorbance spectrum similar to normal rhodopsin, however, G338E mutant green opsin gave no absorbance.[37] We speculate that the molecular mechanisms of R330Q and G338E malfunction can be due to a combination of altered physical property and composition of cone outer segments and abnormal light signaling.

Our conclusions of the disease mechanisms caused by these mutants are based on the assumption that splicing is not affected by any of the missense mutations, as we used AAV to deliver cDNA for each mutant. However, studies have shown that about 15% of single nucleotide substitutions are expected to cause or modify human genetic diseases through mis-splicing,[61–63] and missense mutations in rhodopsin have been shown to exert a major effect on splicing.[64,65] Therefore, in future studies, it is necessary to analyze these missense mutations at the mRNA level in order to rule out this possibility.

4.3 | Treatment strategies

Previously, we have shown that AAV-mediated gene replacement therapy can rescue M-cone function and structure in *Opn1mw*$^{-/-}$ mice, a mouse model representing BCM patients with deletion mutations.[39] However, for cone opsin mutants that display a dominant phenotype, they may need different approaches. A previous study showed that delivery of wild-type rod opsin retarded retinal degeneration in autosomal RP caused by P23H mutation suggesting that increased production of normal rhodopsin can suppress the effect of the mutated protein.[66] Such an approach may be helpful for cone opsin mutants with a dominant phenotype and needs to be tested in individual knock-in mouse models. However, we need to carefully evaluate the consequence of a potential toxic gain-of-function or dominant-negative effect of the mutant protein on the wild-type opsin introduced into cells harboring a preexisting misfolded/mistargeted cone opsin mutation. Alternatively, shRNA delivery to knock down the level of mutant cone opsin expression in combination with supplementation of a "harden" (shRNA resistant) copy of normal *OPN1LW* cDNA might be a better option. Such an approach has been successfully used to treat autosomal-dominant RP associated with rhodopsin in mouse and canine models.[67,68] Recently, several studies have also demonstrated success in the correction of rhodopsin-associated autosomal-dominant RP by CRISPR/Cas9 gene editing,[69–71] and this may also represent a viable approach to treat dominant cone opsin mutations as well. Third, for misfolded proteins, such as N94K and W177R, the presence of high levels of misfolded protein in the ER upregulates the unfolded protein response (UPR). Modulation of UPR by targeting key components of the different branches of the pathway has been shown to reduce ER stress and prevent photoreceptor cell death.[72]

In summary, we performed the first in vivo study to elucidate the molecular mechanisms underlying five cone opsin missense mutations associated with cone dystrophy/dysfunction. We conclude that although each point mutation displays a distinct consequence on cone opsin structure and function, all appear to present dominant phenotypes. Understanding the molecular mechanisms associated with these cone opsin mutants offers the potential for the development of targeted therapies for this currently untreatable form of retinal neurodegeneration.

ACKNOWLEDGMENTS

We thank Drs Arshavsky and Lobanova (Department of Ophthalmology, Duke University School of Medicine) for kindly provided us with cone transducin γ subunit antibody. This work was supported by the National Institutes of Health (R01 EY030056 to Deng, EY021721 to Hauswirth, R01 EY08123 to Baehr), National Eye Institute (EY014800-039003, core grant to the Department of Ophthalmology, University of Utah), unrestricted grants to the Departments of Ophthalmology at the University of Florida and the University of Utah from Research to Prevent Blindness (RPB; New York), and SIG grant National Institutes of Health (1S10OD028476 to Department of Ophthalmology, University of Florida).

DISCLOSURES

WWH and the University of Florida have a financial interest in the use of AAV therapies, and WWH owns equity in a company (AGTC Inc.) that might, in the future, commercialize some aspects of this work.

AUTHOR CONTRIBUTIONS

Deng WT designed research; Zhu P, Dyka F, Ma Xi, Yin L, Deng WT, and Yu H performed research; Deng WT, Baehr W, and Hauswirth WW analyzed data; Deng WT, Baehr W and Hauswirth WW wrote the paper.

ORCID

Wen-Tao Deng https://orcid.org/0000-0002-9357-0656

REFERENCES

1. Curcio CA, Allen KA, Sloan KR, et al. Distribution and morphology of human cone photoreceptors stained with anti-blue opsin. *J Comp Neurol*. 1991;312:610-624.
2. Curcio CA, Sloan KR, Kalina RE, Hendrickson AE. Human photoreceptor topography. *J Comp Neurol*. 1990;292:497-523.
3. Mustafi D, Engel AH, Palczewski K. Structure of cone photoreceptors. *Prog Retin Eye Res*. 2009;28:289-302.
4. Nathans J, Thomas D, Hogness DS. Molecular genetics of human color vision: the genes encoding blue, green, and red pigments. *Science*. 1986;232:193-202.
5. Ayyagari R, Kakuk LE, Coats CL, et al. Bilateral macular atrophy in blue cone monochromacy (BCM) with loss of the locus control region (LCR) and part of the red pigment gene. *Mol Vis*. 1999;5:13.
6. Carroll J, Baraas RC, Wagner-Schuman M, et al. Cone photoreceptor mosaic disruption associated with Cys203Arg mutation in the M-cone opsin. *Proc Natl Acad Sci U S A*. 2009;106:20948-20953.
7. Carroll J, Neitz M, Hofer H, Neitz J, Williams DR. Functional photoreceptor loss revealed with adaptive optics: an alternate cause of color blindness. *Proc Natl Acad Sci U S A*. 2004;101:8461-8466.
8. Crognale MA, Fry M, Highsmith J, et al. Characterization of a novel form of X-linked incomplete achromatopsia. *Vis Neurosci*. 2004;21:197-203.
9. Gardner JC, Michaelides M, Holder GE, et al. Blue cone monochromacy: causative mutations and associated phenotypes. *Mol Vis*. 2009;15:876-884.
10. Gardner JC, Webb TR, Kanuga N, et al. X-linked cone dystrophy caused by mutation of the red and green cone opsins. *Am J Hum Genet*. 2010;87:26-39.
11. Jagla WM, Jagle H, Hayashi T, Sharpe LT, Deeb SS. The molecular basis of dichromatic color vision in males with multiple red and green visual pigment genes. *Hum Mol Genet*. 2002;11:23-32.
12. Kellner U, Wissinger B, Tippmann S, Kohl S, Kraus H, Foerster MH. Blue cone monochromatism: clinical findings in patients with mutations in the red/green opsin gene cluster. *Graefes Arch Clin Exp Ophthalmol*. 2004;242:729-735.
13. Michaelides M, Johnson S, Bradshaw K, et al. X-linked cone dysfunction syndrome with myopia and protanopia. *Ophthalmology*. 2005;112:1448-1454.
14. Michaelides M, Johnson S, Simunovic MP, et al. Blue cone monochromatism: a phenotype and genotype assessment with evidence of progressive loss of cone function in older individuals. *Eye (Lond)*. 2005;19:2-10.
15. Mizrahi-Meissonnier L, Merin S, Banin E, Sharon D. Variable retinal phenotypes caused by mutations in the X-linked photopigment gene array. *Invest Ophthalmol Vis Sci*. 2010;51:3884-3892.
16. Nathans J, Davenport C, Maumenee I, et al. Molecular genetics of human blue cone monochromacy. *Science*. 1989;245:831-838.
17. Nathans J, Maumenee IH, Zrenner E, et al. Genetic heterogeneity among blue-cone monochromats. *Am J Hum Genet*. 1993;53:987-1000.
18. Neitz M, Carroll J, Renner A, Knau H, Werner JS, Neitz J. Variety of genotypes in males diagnosed as dichromatic on a conventional clinical anomaloscope. *Vis Neurosci*. 2004;21:205-216.
19. Winderickx J, Sanocki E, Lindsey DT, Teller DY, Motulsky AG, Deeb SS. Defective colour vision associated with a missense mutation in the human green visual pigment gene. *Nat Genet*. 1992;1:251-256.
20. Neitz J, Neitz M. The genetics of normal and defective color vision. *Vision Res*. 2011;51:633-651.
21. Reyniers E, Van Thienen MN, Meire F, et al. Gene conversion between red and defective green opsin gene in blue cone monochromacy. *Genomics*. 1995;29:323-328.
22. Deeb SS, Lindsey DT, Hibiya Y, et al. Genotype-phenotype relationships in human red/green color-vision defects: molecular and psychophysical studies. *Am J Hum Genet*. 1992;51:687-700.
23. Nathans J, Piantanida TP, Eddy RL, Shows TB, Hogness DS. Molecular genetics of inherited variation in human color vision. *Science*. 1986;232:203-210.
24. Buena-Atienza E, Ruther K, Baumann B, et al. De novo intrachromosomal gene conversion from OPN1MW to OPN1LW in the male germline results in blue cone monochromacy. *Sci Rep*. 2016;6:28253.
25. Carroll J, Dubra A, Gardner JC, et al. The effect of cone opsin mutations on retinal structure and the integrity of the photoreceptor mosaic. *Invest Ophthalmol Vis Sci*. 2012;53:8006-8015.
26. Carroll J, Rossi EA, Porter J, et al. Deletion of the X-linked opsin gene array locus control region (LCR) results in disruption of the cone mosaic. *Vision Res*. 2010;50:1989-1999.
27. Cideciyan AV, Hufnagel RB, Carroll J, et al. Human cone visual pigment deletions spare sufficient photoreceptors to warrant gene therapy. *Hum Gene Ther*. 2013;24:993-1006.

28. Gardner JC, Liew G, Quan YH, et al. Three different cone opsin gene array mutational mechanisms with genotype-phenotype correlation and functional investigation of cone opsin variants. *Hum Mutat*. 2014;35:1354-1362.
29. Greenwald SH, Kuchenbecker JA, Rowlan JS, Neitz J, Neitz M. Role of a dual splicing and amino acid code in myopia, cone dysfunction and cone dystrophy associated with L/M opsin interchange mutations. *Transl Vis Sci Technol*. 2017;6:2.
30. Orosz O, Rajta I, Vajas A, et al. Myopia and late-onset progressive cone dystrophy associate to LVAVA/MVAVA Exon 3 interchange haplotypes of opsin genes on chromosome X. *Invest Ophthalmol Vis Sci*. 2017;58:1834-1842.
31. Ueyama H, Muraki-Oda S, Yamade S, et al. Unique haplotype in exon 3 of cone opsin mRNA affects splicing of its precursor, leading to congenital color vision defect. *Biochem Biophys Res Commun*. 2012;424:152-157.
32. Sumaroka A, Garafalo AV, Cideciyan AV, et al. Blue cone monochromacy caused by the C203R missense mutation or large deletion mutations. *Invest Ophthalmol Vis Sci*. 2018;59:5762-5772.
33. Kazmi MA, Sakmar TP, Ostrer H. Mutation of a conserved cysteine in the X-linked cone opsins causes color vision deficiencies by disrupting protein folding and stability. *Invest Ophthalmol Vis Sci*. 1997;38:1074-1081.
34. Hwa J, Reeves PJ, Klein-Seetharaman J, Davidson F, Khorana HG. Structure and function in rhodopsin: further elucidation of the role of the intradiscal cysteines, Cys-110, -185, and -187, in rhodopsin folding and function. *Proc Natl Acad Sci U S A*. 1999;96:1932-1935.
35. Mendes HF, van der Spuy J, Chapple JP, Cheetham ME. Mechanisms of cell death in rhodopsin retinitis pigmentosa: implications for therapy. *Trends Mol Med*. 2005;11:177-185.
36. Ostrer H, Kazmi MA. Mutation of a conserved proline disrupts the retinal-binding pocket of the X-linked cone opsins. *Mol Vis*. 1997;3:16.
37. Ueyama H, Kuwayama S, Imai H, et al. Novel missense mutations in red/green opsin genes in congenital color-vision deficiencies. *Biochem Biophys Res Commun*. 2002;294:205-209.
38. Srinivasan S, Fernandez-Sampedro MA, Ramon E, Garriga P. Structural and functional alterations associated with deutan N94K and R330Q mutations of green cone opsin. *Biochim Biophys Acta*. 2017;1863:1840-1847.
39. Deng WT, Li J, Zhu P, et al. Human L- and M-opsins restore M-cone function in a mouse model for human blue cone monochromacy. *Mol Vis*. 2018;24:17-28.
40. Zhang Y, Deng WT, Du W, et al. Gene-based therapy in a mouse model of blue cone monochromacy. *Sci Rep*. 2017;7:6690.
41. Mancuso K, Hauswirth WW, Li Q, et al. Gene therapy for red-green colour blindness in adult primates. *Nature*. 2009;461:784-787.
42. Zolotukhin S, Potter M, Zolotukhin I, et al. Production and purification of serotype 1, 2, and 5 recombinant adeno-associated viral vectors. *Methods*. 2002;28:158-167.
43. Pang JJ, Boye SL, Kumar A, et al. AAV-mediated gene therapy for retinal degeneration in the rd10 mouse containing a recessive PDEbeta mutation. *Invest Ophthalmol Vis Sci*. 2008;49:4278-4283.
44. Pang JJ, Chang B, Kumar A, et al. Gene therapy restores vision-dependent behavior as well as retinal structure and function in a mouse model of RPE65 Leber congenital amaurosis. *Mol Ther*. 2006;13:565-572.
45. Stenkamp RE, Filipek S, Driessen CA, Teller DC, Palczewski K. Crystal structure of rhodopsin: a template for cone visual pigments and other G protein-coupled receptors. *Biochim Biophys Acta*. 2002;1565:168-182.
46. Jones BW, Kondo M, Terasaki H, et al. Retinal remodeling in the Tg P347L rabbit, a large-eye model of retinal degeneration. *J Comp Neurol*. 2011;519:2713-2733.
47. Hofmann L, Alexander NS, Sun W, Zhang J, Orban T, Palczewski K. Hydrogen/deuterium exchange mass spectrometry of human green opsin reveals a conserved pro-pro motif in extracellular loop 2 of monostable visual G protein-coupled receptors. *Biochemistry*. 2017;56:2338-2348.
48. Vissers PM, DeGrip WJ. Functional expression of human cone pigments using recombinant baculovirus: compatibility with histidine tagging and evidence for N-glycosylation. *FEBS Lett*. 1996;396:26-30.
49. Ostrer H, Pullarkat RK, Kazmi MA. Glycosylation and palmitoylation are not required for the formation of the X-linked cone opsin visual pigments. *Mol Vis*. 1998;4:28.
50. Kirchberg K, Kim TY, Moller M, et al. Conformational dynamics of helix 8 in the GPCR rhodopsin controls arrestin activation in the desensitization process. *Proc Natl Acad Sci U S A*. 2011;108:18690-18695.
51. Deming JD, Pak JS, Shin JA, et al. Arrestin 1 and Cone Arrestin 4 have unique roles in visual function in an all-cone mouse retina. *Invest Ophthalmol Vis Sci*. 2015;56:7618-7628.
52. Blanks JC, Johnson LV. Selective lectin binding of the developing mouse retina. *J Comp Neurol*. 1983;221:31-41.
53. Athanasiou D, Aguila M, Bellingham J, et al. The molecular and cellular basis of rhodopsin retinitis pigmentosa reveals potential strategies for therapy. *Prog Retin Eye Res*. 2018;62:1-23.
54. Nemet I, Ropelewski P, Imanishi Y. Rhodopsin trafficking and mistrafficking: signals, molecular components, and mechanisms. *Prog Mol Biol Transl Sci*. 2015;132:39-71.
55. Park PS. Constitutively active rhodopsin and retinal disease. *Adv Pharmacol*. 2014;70:1-36.
56. Sohocki MM, Daiger SP, Bowne SJ, et al. Prevalence of mutations causing retinitis pigmentosa and other inherited retinopathies. *Hum Mutat*. 2001;17:42-51.
57. Sullivan LS, Bowne SJ, Birch DG, et al. Prevalence of disease-causing mutations in families with autosomal dominant retinitis pigmentosa: a screen of known genes in 200 families. *Invest Ophthalmol Vis Sci*. 2006;47:3052-3064.
58. Zhang F, Zhang Q, Shen H, Li S, Xiao X. Analysis of rhodopsin and peripherin/RDS genes in Chinese patients with retinitis pigmentosa. *Yan Ke Xue Bao*. 1998;14:210-214.
59. Rivera-De la Parra D, Cabral-Macias J, Matias-Florentino M, et al. N78I dominant mutation causing sectorial retinitis pigmentosa in a pedigree with intrafamilial clinical heterogeneity. *Gene*. 2013;519 173-176.
60. Yoshizawa T. The road to color vision: structure, evolution and function of chicken and gecko visual pigments. *Photochem Photobiol*. 1992;56:859-867.
61. Baralle D, Baralle M. Splicing in action: assessing disease causing sequence changes. *J Med Genet*. 2005;42:737-748.
62. Faustino NA, Cooper TA. Pre-mRNA splicing and human disease. *Genes Dev*. 2003;17:419-437.
63. Wang GS, Cooper TA. Splicing in disease: disruption of the splicing code and the decoding machinery. *Nat Rev Genet*. 2007;8:749-761.

64. Riedmayr LM, Bohm S, Biel M, Becirovic E. Enigmatic rhodopsin mutation creates an exceptionally strong splice acceptor site. *Hum Mol Genet*. 2020;29:295-304.
65. Tanner G, Glaus E, Barthelmes D, et al. Therapeutic strategy to rescue mutation-induced exon skipping in rhodopsin by adaptation of U1 snRNA. *Hum Mutat*. 2009;30:255-263.
66. Mao H, James T Jr, Schwein A, et al. AAV delivery of wild-type rhodopsin preserves retinal function in a mouse model of autosomal dominant retinitis pigmentosa. *Hum Gene Ther*. 2011;22:567-575.
67. Mao H, Gorbatyuk MS, Rossmiller B, Hauswirth WW, Lewin AS. Long-term rescue of retinal structure and function by rhodopsin RNA replacement with a single adeno-associated viral vector in P23H RHO transgenic mice. *Hum Gene Ther*. 2012;23:356-366.
68. Cideciyan AV, Sudharsan R, Dufour VL, et al. Mutation-independent rhodopsin gene therapy by knockdown and replacement with a single AAV vector. *Proc Natl Acad Sci U S A*. 2018;115:E8547-E8556.
69. Bakondi B, Lv W, Lu B, et al. In vivo CRISPR/Cas9 gene editing corrects retinal dystrophy in the S334ter-3 rat model of autosomal dominant retinitis pigmentosa. *Mol Ther*. 2016;24:556-563.
70. Giannelli SG, Luoni M, Castoldi V, et al. Cas9/sgRNA selective targeting of the P23H Rhodopsin mutant allele for treating retinitis pigmentosa by intravitreal AAV9.PHP.B-based delivery. *Hum Mol Genet*. 2018;27:761-779.
71. Li P, Kleinstiver BP, Leon MY, et al. Allele-specific CRISPR-Cas9 genome editing of the single-base P23H mutation for rhodopsin-associated dominant retinitis pigmentosa. *CRISPR J*. 2018;1:55-64.
72. Griciuc A, Aron L, Ueffing M. ER stress in retinal degeneration: a target for rational therapy? *Trends Mol Med*. 2011;17:442-451.

SUPPORTING INFORMATION

Additional supporting information may be found online in the Supporting Information section.

How to cite this article: Zhu P, Dyka F, Ma X, et al. Disease mechanisms of X-linked cone dystrophy caused by missense mutations in the red and green cone opsins. *FASEB J*. 2021;35:e21927. doi:10.1096/fj.202101066R